

Higher-order nonlinear Schrödinger equation with derivative non-Kerr nonlinear terms: A model for sub-10-fs-pulse propagation

Amitava Choudhuri^{1,*} and K. Porsezian²¹*Department of Astrophysics, School of Physical, Chemical and Applied Sciences, Pondicherry University, Pondicherry 605014, India*²*Department of Physics, School of Physical, Chemical and Applied Sciences, Pondicherry University, Pondicherry 605014, India*

(Received 13 May 2013; revised manuscript received 12 August 2013; published 4 September 2013)

We analytically solve the higher-order nonlinear Schrödinger (HNLS) equation with non-Kerr nonlinearity under some parametric conditions and obtain results for bright and dark solitary wave solutions. The functional form of these solutions are different from the traditional sech and tanh bright and dark solitons. Periodic wave solutions are also presented. Going over to the traveling coordinate, we reduce the complicated HNLS equation to the Hamiltonian form and treat the resulting equations by the dynamical systems theory. The results of our study demonstrate that the equation can, in general, support both soliton (bright and dark) and periodic solutions. We estimate the size of the derivative non-Kerr nonlinear coefficients. The results are in good agreement with those of the waveguide made of highly nonlinear optical materials. Our calculated values can be used as model parameters for sub-10 fs pulse propagation.

DOI: [10.1103/PhysRevA.88.033808](https://doi.org/10.1103/PhysRevA.88.033808)

PACS number(s): 42.81.Dp, 05.45.Yv, 42.65.Tg, 42.79.Sz

I. INTRODUCTION

Optical solitons have potential to become principal information carriers in telecommunication due to their capability of propagating long distances without attenuation and change in shape. Consequently, many theoretical and experimental studies were envisaged to analyze the dynamics of solitons in an optical waveguide. The waveguides used in the picosecond pulse propagation in nonlinear optical communication systems are usually of Kerr type. Here the dynamics of light pulses are described by the nonlinear Schrödinger (NLS) family of equations with cubic nonlinearity [1]. The validity of the NLS equation as a reliable model is dependent on the assumption that the spatial width of the soliton is much larger than the carrier wavelength. In other words, we require the width of the soliton frequency to be much less than that of the carrier frequency. While the robustness of the optical soliton makes it useful for long distance optical communication, the high frequency of the carrier wave generates high bit rates. To increase the bit rate further it is often desirable to use shorter femtosecond pulses (< 100 fs). The propagation of such short wavelength pulses through waveguides having negligible fiber loss is modeled by a higher order nonlinear Schrödinger equation (HNLS) [2]:

$$E_z = i(a_1 E_{tt} + a_2 |E|^2 E) + a_3 E_{ttt} + a_4 (|E|^2 E)_t + a_5 E (|E|^2)_t. \quad (1)$$

Here z is the normalized distance along the fiber and t is the normalized time with the frame of the reference moving along the fiber at the group velocity. The subscripts z and t denote the spatial and temporal partial derivatives respectively. The coefficients a_i ($i = 1, 2, \dots, 5$), particularly, $a_1 = \frac{\beta_2}{2}$, $a_2 = \gamma_1$, $a_3 = \frac{\beta_3}{6}$, $a_4 = -\frac{\gamma_1}{\omega_0}$, and $a_5 = \gamma_1 T_R$, are the real parameters related to group velocity dispersion (GVD), self-phase modulation (SPM), third-order dispersion (TOD), self steepening, and self-frequency shift due to stimulated Raman

scattering (SRS) respectively. Here $\beta_j = (\frac{d^j \beta}{d\omega^j})_{\omega=\omega_0}$, the dispersion coefficients evaluated at the carrier frequency ω_0 , with β_1 , the inverse of group velocity, β_2 , the group velocity dispersion parameter, β_3 the third order dispersion (TOD) parameter, and so on. As the fiber dispersion plays a critical role in propagation of short optical pulses because different spectral components associated with the pulse travel at different speeds given by $c/n(\omega)$, we have $\beta = \frac{n(\omega)\omega}{c}$, the mode propagation constant, where $n(\omega)$ is the refractive index and c is the velocity of light. More specifically, γ_1 is a coefficient of cubic nonlinearity, which results from the intensity-dependent refractive index. The term related to $\frac{\gamma_1}{\omega_0}$ results from the intensity dependence of the group velocity and causes self-steepening and shock formation at the pulse edge. The last term related to $a_5 = \gamma_1 T_R$ incorporates the intrapulse Raman scattering and originates from the delayed response, which causes a self-frequency shift. Here the Raman time constant, T_R , can be estimated from the slope of the Raman gain (SRS). The characteristic Raman time constant T_R is defined as the first moment of the nonlinear response function [3]. Actually, to model intrapulse Raman scattering the last coefficient a_5 should be $a_5 = i\gamma_1 T_R$. However, in the present work we succeed in deriving analytical solutions in the case when a_5 is real. That the latter case (a_5 real) also dominates in the analytical studies (Painlevé property, inverse scattering transform, Hirota direct method, conservation laws) undertaken to date [4] to show its integrable nature and obtain different types of exact solutions, e.g., w-shaped solution, bright and dark optical solitary wave solutions, etc. Many recent works [4] represent a significant advance as compared to previous ones, and the extension of the work to the case of a_5 imaginary represents a theoretical challenge that should be undertaken in the near future.

Physical processes in materials and molecules which occur on a femtosecond time scale can be understood using ultrafast lasers with pulses as short as 10 fs. Laser spectroscopic techniques have been widely applied to all fields in science including chemistry, physics, and biology to get an idea about microscopic insights into bulk materials, molecules, as well as

*amitava_ch26@yahoo.com

chemical and biochemical reaction processes, which are still unknown to us exactly. The advances in ultrashort laser pulses technology make it possible to observe the coherent motion of atoms, interaction of electrons with their environment, and phonon dynamics in various molecular systems and bulk materials in femtosecond resolution. In addition to these current applications in telecommunication and ultrafast signal routing systems, as the intensity of the incident light field becomes stronger, non-Kerr nonlinear effects come into play. Due to these additional effects, the physical features and the stability of the NLS soliton can change. The way the non-Kerr nonlinearity influences NLS soliton propagation is described by the HNLS family of equations with higher degree of nonlinear terms [5]. To increase the channel handling capacity and ultra-high-speed pulse, it is necessary to transmit solitary waves at a high bit rate ($\approx 1-10$ fs) of ultrashort pulses, which can be seen in many applicative contexts such as high-repetition pulse sources based on fiber technology [6]. At the same time, it is also important to include some additional higher-order perturbation effects to the HNLS equation to analyze the solitary wave solution in a non-Kerr nonlinear medium.

In this paper we study the bright and dark solitary wave solutions for a HNLS equation that contains the time derivative of non-Kerr nonlinear terms and estimate the size of model coefficients, which will be useful to simulate propagation of very short pulses of width around sub-10 fs in highly nonlinear optical fibers. The paper is organized as follows: Sec. II presents a generalized HNLS equation with derivative non-Kerr nonlinear terms, which describes propagation of very short pulses of width around sub-10 fs in highly nonlinear optical fibers. In Sec. III we present exact solitary wave solutions of our model equation in the form of bright, dark, and periodic solutions. We also present here the phase plane analysis and discuss various results on the existence of above solutions along with the linear stability check. In Sec. IV we present a physical discussion and some applications of our model equation. Finally, in Sec. V we summarize our outlook on the present work and make concluding remarks.

II. MODEL EQUATION

We consider the higher-order NLS (HNLS) equation with non-Kerr term [7], which can be written in terms of a slowly varying complex envelope of the electric field $E(z, t)$, as

$$E_z = i(a_1 E_{tt} + a_2 |E|^2 E) + a_3 E_{ttt} + a_4 (|E|^2 E)_t + a_5 E (|E|^2)_t + i a_6 |E|^4 E + a_7 (|E|^4 E)_t + a_8 E (|E|^4)_t. \quad (2)$$

The terms related to coefficients a_6, a_7, a_8 in Eq. (2) represent the quintic non-Kerr nonlinearities. The quintic nonlinearities arise from the expansion of the refractive index in power of intensity I of the light pulse: $n = n_0 + n_2 I + n_4 I^2 + \dots$. Here n_0 is the linear refractive index and n_2, n_4 are the nonlinear refractive indices and originate from third- and fifth-order susceptibilities respectively. The polarizations induced through these susceptibilities give the cubic and quintic (non-Kerr) terms in a nonlinear Schrödinger equation. The nonlinearity that arises due to fifth-order susceptibility can be obtained in many optical materials such as semiconductors,

semiconductor doped glasses, AlGaAs, polydiacetylene toluene sulfonate (PTS), chalcogenide glasses, and some transparent organic materials. When the last three terms related to a_6, a_7, a_8 in Eq. (2) are ignored, the resulting equation becomes the HNLS equation as given in Eq. (1). In a recent paper [7] we investigated the dark-in-the-bright (DITB) solitary wave solution of Eq. (2). The DS or DITB solitary wave solution is composed of the product of bright and dark solitary waves. We also investigated the stability of the DITB solution under some initial perturbation on the parametric conditions. The shape of the pulse remains unchanged up to 20 normalized lengths even under some very small violation in parametric conditions. More recently [8], we studied the modulational instability (MI) of Eq. (2) with fourth-order dispersion in the context of optics and presented an analytical expression for MI gain to show the effects of non-Kerr nonlinearities and higher-order dispersions on MI gain spectra. In our study we also demonstrated that MI can exist not only for an anomalous group velocity dispersion (GVD) regime but also in the normal GVD regime. We further investigated that the quintic non-Kerr nonlinear terms are more important than the cubic Kerr nonlinearity because non-Kerr nonlinearities are responsible for stability of localized solutions. But in the previous works [5,7,8] the solitary wave solutions in the presence of higher non-Kerr nonlinearity have not been investigated. In a very recent work, Triki and Taha [9] presented solitary wave solutions for the HNLS equation including non-Kerr nonlinear terms up to the coefficient a_6 of Eq. (2).

III. SOLITARY WAVE SOLUTIONS AND PHASE PLANE ANALYSIS

To investigate the existence of analytic wave solution of the HNLS equation in the presence of non-Kerr terms we begin by scaling the variables of the Eq. (2) in the form

$$E = b_1 \Psi, \quad z = b_2 \xi, \quad \text{and} \quad t = b_3 \tau$$

and choosing b_1, b_2 , and b_3 such that the coefficients corresponding to GVD, SPM, and TOD become unity. Thus in the scaled form of the Eq. (2) becomes

$$\Psi_\xi = i(\Psi_{\tau\tau} + |\Psi|^2 \Psi) + \Psi_{\tau\tau\tau} + \alpha_1 (|\Psi|^2 \Psi)_\tau + \alpha_2 \Psi (|\Psi|^2)_\tau + i \alpha_3 |\Psi|^4 \Psi + \alpha_4 (|\Psi|^4 \Psi)_\tau + \alpha_5 \Psi (|\Psi|^4)_\tau, \quad (3)$$

where

$$\alpha_1 = \frac{b_1^2 b_2 a_4}{b_3} = \frac{a_4 a_1}{a_2 a_3}, \quad \alpha_2 = \frac{b_1^2 b_2 a_5}{b_3} = \frac{a_5 a_1}{a_2 a_3},$$

$$\alpha_3 = b_1^4 b_2 a_6 = \frac{a_6 a_1^3}{a_2^2 a_3}, \quad \alpha_4 = \frac{b_1^4 b_2 a_7}{b_3} = \frac{a_7 a_1^4}{a_2^2 a_3}, \quad \text{and}$$

$$\alpha_5 = \frac{b_1^4 b_2 a_8}{b_3} = \frac{a_8 a_1^4}{a_2^2 a_3}.$$

In writing (3) we have chosen $b_1 = (\frac{a_1^3}{a_2^2 a_3})^{\frac{1}{2}}$, $b_2 = \frac{a_2^2}{a_1}$, and $b_3 = \frac{a_3}{a_1}$.

To obtain the exact solitary wave solutions of Eq. (3) we consider a solution of the form

$$\Psi(\xi, \tau) = \mathcal{P}(\tau + v\xi) e^{i(k\xi - \Omega\tau)} = \mathcal{P}(\chi) e^{i(k\xi - \Omega\tau)}, \quad (4)$$

with $\mathcal{P}(\chi)$ is real and $\chi = \tau + v\xi$ is often referred to as the traveling coordinate. Substituting Eq. (4) into Eq. (3) we will get an equation of which the imaginary part gives a second-order ordinary differential equation, whereas a third-order differential equation results from the real part. Now removing the exponential terms from both the equations and integrating once of the third-order equation, one can obtain the resulting equations as

$$\mathcal{P}_{\chi\chi} = (v - 2\Omega + 3\Omega^2)\mathcal{P} - \frac{3\alpha_1 + 2\alpha_2}{3}\mathcal{P}^3 - \frac{5\alpha_4 + 4\alpha_5}{5}\mathcal{P}^5 \quad (5a)$$

and

$$\mathcal{P}_{\chi\chi} = \frac{(k + \Omega^2 - \Omega^3)}{(1 - 3\Omega)}\mathcal{P} - \frac{(1 - \Omega\alpha_1)}{(1 - 3\Omega)}\mathcal{P}^3 - \frac{(\alpha_3 - \Omega\alpha_4)}{(1 - 3\Omega)}\mathcal{P}^5. \quad (5b)$$

Equations (5a) and (5b) are identical if we equate the coefficients of \mathcal{P} , \mathcal{P}^3 , and \mathcal{P}^5 .

Before deriving explicit localized solutions, we shall carry out a qualitative analysis of the second-order ordinary differential equation obtain from (5a) written as

$$\frac{d^2\mathcal{P}}{d\chi^2} = a\mathcal{P} - 2b\mathcal{P}^3 - 3c\mathcal{P}^5. \quad (6)$$

Now multiplying (6) by \mathcal{P}_χ and integrating we get

$$(\mathcal{P}_\chi)^2 = a\mathcal{P}^2 - b\mathcal{P}^4 - c\mathcal{P}^6 + 2\mathcal{E}, \quad (7)$$

where $a = (v - 2\Omega + 3\Omega^2)$, $b = \frac{3\alpha_1 + 2\alpha_2}{6}$, $c = \frac{5\alpha_4 + 4\alpha_5}{15}$, and \mathcal{E} is the arbitrary constant of integration. Equation (6) describes the evolution of the anharmonic oscillator with potential

$$U(\mathcal{P}) = -\frac{a}{2}\mathcal{P}^2 + \frac{b}{2}\mathcal{P}^4 + \frac{c}{2}\mathcal{P}^6. \quad (8)$$

Equation (6) can be represented by two equivalent first-order differential equations given by

$$\frac{d\mathcal{P}}{d\chi} = \mathcal{Q} = p(\mathcal{P}, \mathcal{Q}) \quad (\text{say}) \quad (9a)$$

and

$$\frac{d\mathcal{Q}}{d\chi} = a\mathcal{P} - 2b\mathcal{P}^3 - 3c\mathcal{P}^5 = q(\mathcal{P}, \mathcal{Q}) \quad (\text{say}). \quad (9b)$$

It is rather straightforward to show that Eqs. (9a) and (9b) form a Hamiltonian system, satisfying the canonical equations

$$\frac{d\mathcal{P}}{d\chi} = \frac{\partial H}{\partial \mathcal{Q}} \quad \text{and} \quad \frac{d\mathcal{Q}}{d\chi} = -\frac{\partial H}{\partial \mathcal{P}}, \quad (10)$$

with the integration constant \mathcal{E} given in Eq. (7) as the Hamiltonian H of the dynamical system described by Eq. (6). We obtained five equilibrium points $(\mathcal{P}_i^*, \mathcal{Q}_i^*)$ ($i = 1, \dots, 5$) of Eq. (10) by solving $\frac{d\mathcal{P}}{d\chi} = 0$ and $\frac{d\mathcal{Q}}{d\chi} = 0$. These are

$$\begin{aligned} & \left(-\sqrt{-\frac{b}{3c} - \frac{\sqrt{b^2+3ac}}{3c}}, 0\right), & \left(-\sqrt{-\frac{b}{3c} + \frac{\sqrt{b^2+3ac}}{3c}}, 0\right), \\ & (0, 0), & \\ & \left(\sqrt{-\frac{b}{3c} + \frac{\sqrt{b^2+3ac}}{3c}}, 0\right), & \left(\sqrt{-\frac{b}{3c} - \frac{\sqrt{b^2+3ac}}{3c}}, 0\right). \end{aligned}$$

As we have written the equation in the form of (9), following the general criteria for the linear stability analysis, we now make use of the eigenvalues of the Jacobian matrix [10]

$$\mathcal{M} = \begin{pmatrix} T_1 & T_2 \\ T_3 & T_4 \end{pmatrix}, \quad \det \mathcal{M} \neq 0 \quad (11)$$

to disclose the relationship between the critical points and the solutions supported by Eq. (6). We can construct the elements of the matrix in Eq. (11) by using

$$\begin{aligned} T_1 &= \frac{\partial p}{\partial \mathcal{P}}|_{(\mathcal{P}^*, \mathcal{Q}^*)}, & T_2 &= \frac{\partial p}{\partial \mathcal{Q}}|_{(\mathcal{P}^*, \mathcal{Q}^*)}, \\ T_3 &= \frac{\partial q}{\partial \mathcal{P}}|_{(\mathcal{P}^*, \mathcal{Q}^*)}, & T_4 &= \frac{\partial q}{\partial \mathcal{Q}}|_{(\mathcal{P}^*, \mathcal{Q}^*)}. \end{aligned}$$

Here $(\mathcal{P}_i^*, \mathcal{Q}_i^*)$ stands for the critical points. In the following we will discuss two cases.

A. Case 1: $\Omega \neq \frac{1}{3}$

Equating (5a) and (5b) we get the following necessary and sufficient conditions on Ω and equation for k in terms of Ω :

$$\Omega = \frac{3\alpha_1 + 2\alpha_2 - 3}{6(\alpha_1 + \alpha_2)} = \frac{5\alpha_4 + 4\alpha_5 - 5\alpha_3}{(10\alpha_4 + 12\alpha_5)} \quad (12a)$$

and

$$k = (1 - 3\Omega)(v - 2\Omega + 3\Omega^2) - \Omega^2 + \Omega^3 \quad (12b)$$

with constraint relations

$$\alpha_4 = \frac{3\alpha_1}{5}, \quad \alpha_5 = \frac{\alpha_2}{2}, \quad \text{and} \quad \alpha_3 = \frac{3}{5}. \quad (13)$$

For zero energy ($\mathcal{E} = 0$) we have found the solution of Eq. (7) as

$$\mathcal{P}(\chi) = \frac{2a^{\frac{3}{4}}\sqrt{(\sqrt{a} - b e^{2\sqrt{a}\chi})^2 + 4ac} e^{4\sqrt{a}\chi} e^{\sqrt{a}\chi}}{\sqrt{[a - (b^2 - 4ac)e^{4\sqrt{a}\chi}]^2 + 16ab^2c e^{8\sqrt{a}\chi}}}, \quad (14)$$

provided that $a > 0$, $b > 0$. Now using Eqs. (4), (12b), and (14) we can write the solution of Eq. (3) as

$$\Psi(\xi, \tau) = \mathcal{P}(\tau + v\xi) e^{i[(1-3\Omega)(v-2\Omega+3\Omega^2)-\Omega^2+\Omega^3]\xi - \Omega\tau}. \quad (15)$$

The intensity profile of the solitary wave solution [Eq. (15)] is shown in Fig. 1(a), as computed from Eq. (3) for the values $a = v = 1.6999$, $b = \frac{1}{2}$, and $c = \frac{1}{5}$. One can check the evolution of the intensity profile. It is interesting to note that the wave profile remains unchanged during evolution, which we have shown in Fig. 1(b). For a negative value of the parameter a , Eq. (3) supports the periodic solution. We have shown the periodic wave solution profile and its evolution in Figs. 2(a) and 2(b). Here we have taken the same parameter values as that in Fig. 1 but $v = -1$ such that $a < 0$. Thus we have seen for $\Omega = 0$ (i.e., $3\alpha_1 + 2\alpha_2 = 3$), and consequently, $a = v$, Eq. (3) supports the bright solitary wave solution ($a > 0$) and periodic solution ($a < 0$) respectively. We can easily check the existence of bright and periodic solutions by using the phase plane analysis. For ($a = 1.6999$, $b = \frac{1}{2}$, and $c = \frac{1}{5}$), the real critical points $(\mathcal{P}_i^*, \mathcal{Q}_i^*)$ are $(-1.02218, 0)$, $(0, 0)$, and $(1.02218, 0)$. Using the general criteria for the linear stability analysis, we have checked from the eigenvalues of the Jacobian matrix in Eq. (11) that

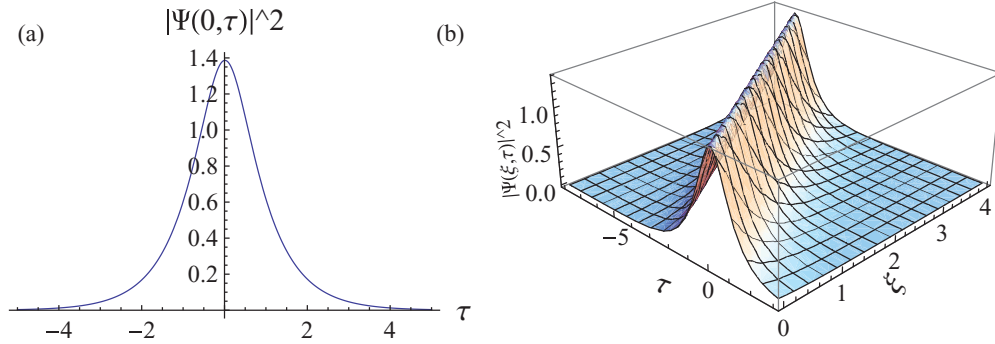


FIG. 1. (Color online) (a) Intensity of the solitary wave profile $|\Psi(0, \tau)|^2$ as a function of τ and its (b) evolution as computed from Eq. (15) for the values $a = v = 1.6999$ and $b = \frac{1}{2}$ and $c = \frac{1}{5}$.

the equilibrium point $(0, 0)$ is a saddle or hyperbolic type and $(\pm 1.02218, 0)$ represents elliptic equilibrium points, also called centers. A numerically computed phase trajectory near the equilibrium points $(-1.02218, 0)$, $(0, 0)$, and $(1.02218, 0)$ is shown in Fig. 3(a), which corresponds to center, saddle, and center, respectively, as expected. It is apparent that between the external (phase curve A) and internal closed orbits (curve C) there exists a phase path which joins the equilibrium points $(0, 0)$ to itself [denoted by path B in Fig. 3(a)] and is a form of separatrix known as a homoclinic orbit. The separatrix is the curve that separates the phase space into two distinct areas. The homoclinic orbit that enters or emerges from the saddle point $(0, 0)$ represents the bright solitary wave solution to the equation which we have shown in Fig. 1(a). For this choice, the potential of the system is of double-well nature with minima at $\mathcal{P} = \pm 1.02218$ and a local maximum at $\mathcal{P} = 0$, have been shown in Fig. 3(b).

It is also interesting to see from the dynamical system analysis that for the value $a < 0$ the eigenvalues of the Jacobian matrix in Eq. (11) for the equilibrium point $(0, 0)$ are purely imaginary, and the point represents the center or elliptic equilibrium point, and the closed phase plot shown in Fig. 4(a) corresponds to periodic solution, which we have shown in Fig. 2(a). Also, as expected, for this choice, the potential of the system is of single-well nature with minimum at $\mathcal{P} = 0$ as can be seen from Fig. 4(b).

Dark solitary wave: We have seen for $\mathcal{E} = 0$, the HNLS equation in the presence of non-Kerr terms supports the bright

optical wave solution provided that the parameter a in Eq. (7) is positive. Now we chose $\mathcal{E} = -\frac{a^2}{6b}$ and $c = -\frac{b^2}{3a}$ such that we can write Eq. (7) in the form

$$d\chi = \left(-\frac{(a - b\mathcal{P}^2)^3}{3ab} \right)^{-\frac{1}{2}} d\mathcal{P}. \quad (16)$$

Integrating Eq. (16) we find

$$\mathcal{P}(\chi) = \frac{a\chi}{\sqrt{b}\sqrt{-3 + a\chi^2}}. \quad (17)$$

Thus we can write the solitary wave solution of Eq. (3), with the same constraint relations stated in (13), as

$$\Psi(\xi, \tau) = \frac{a(\tau + v\xi)}{\sqrt{b}\sqrt{[-3 + a(\tau + v\xi)^2]}} e^{i(k\xi - \Omega\tau)} \quad (18)$$

with $k = (1 - 3\Omega)(v - 2\Omega + 3\Omega^2) - \Omega^2 + \Omega^3$, provided $a < 0$, with $v = 2\Omega - 3\Omega^2 - \frac{5}{36}(3\alpha_1 + 2\alpha_2)$. In Fig. 5(a) we have plotted the intensity profile of the optical solitary wave solution with the parameter values and $a = v = -1.23999$, $b = -\frac{1}{2}$, and $c = -\frac{b^2}{3a}$, while Fig. 5(a) depicts its evolution. We call this solution a dark solitary wave in the sense that the intensity profile associated with such a soliton exhibits a dip in a uniform background. and the asymptotic absolute value of $\Psi(\xi, \tau)$ tends toward a constant nonzero value for large values of τ . The existence of a dark soliton can be understood using the phase plane analysis. We can see the nature of phase trajectories from Fig. 6(a) for three values

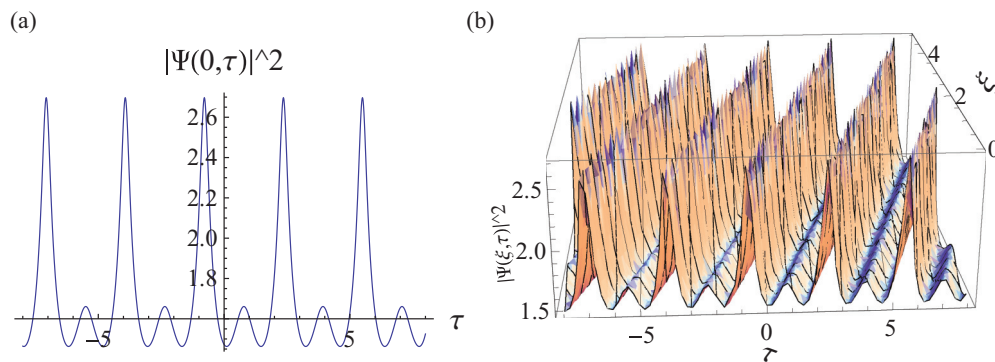


FIG. 2. (Color online) (a) Intensity of the periodic wave profile $|\Psi(0, \tau)|^2$ as a function of τ and its (b) evolution as computed from Eq. (15) for the value $a = v = -1$ and $b = \frac{1}{2}$ and $c = \frac{1}{5}$.

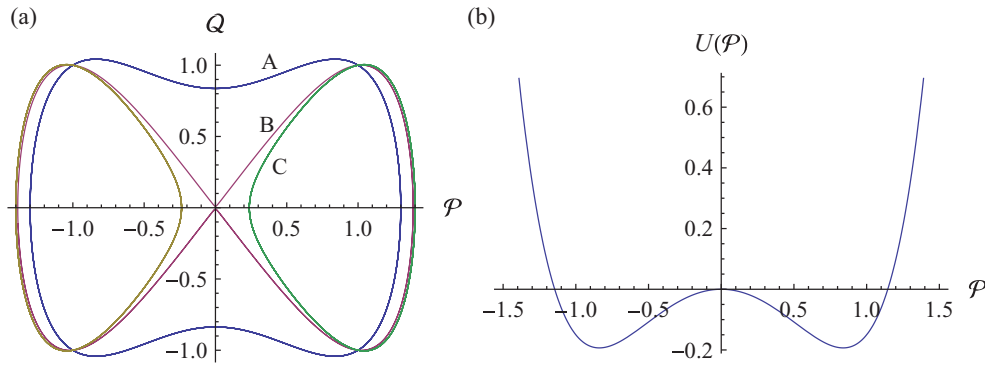


FIG. 3. (Color online) (a) Phase trajectory for the system in Eq. (16). The used parameter values are $a = 1$ (A), $a = 1.6999$ (B), and $a = 1.8$ (C), $b = \frac{1}{2}$, and $c = \frac{1}{5}$ and (b) Shape of the potential function (double-well potential) as computed from Eq. (7) for $a = 1$, $b = \frac{1}{2}$, and $c = \frac{1}{5}$.

of the parameter a , namely, $a = -1.1$, $a = -1.23999$, and $a = -1.6$. We have used the other parameters values as $b = -\frac{1}{2}$ and $c = -\frac{b^2}{3a}$. Following the general criteria for the linear stability analysis, we have checked the eigenvalues of the Jacobian matrix from Eq. (11) for each of the equilibrium points (P_i^*, Q_i^*) using the above three set of values (a, b, c) . In particular, for $(a = -1.1, b = -\frac{1}{2}, c = -0.0757576)$, we have a pair of saddle center overlapping at $(-1.48324, 0)$ and $(1.48324, 0)$ respectively and $(0, 0)$ represents a center. A' in Fig. 6(a) shows the corresponding phase portrait. The phase curve C' represents the periodic curve, and as expected for $(a = -1.6, b = -\frac{1}{2}, c = -0.0520833)$, the only critical point $(0, 0)$ is a center. For the parameter values $(a = -1.23999, b = -\frac{1}{2}, c = -\frac{b^2}{3a})$, the equilibrium points $(\pm 1.5748, 0)$ are of saddle or hyperbolic type, and $(0, 0)$ represents the elliptic equilibrium point, also called the center, and the corresponding phase curve B' is heteroclinic orbit which connects the periodic orbit. In this context, a heteroclinic orbit $x(t)$ refers to a bounding trajectory of a system if there are two distinct saddle

points at x_1^* and x_2^* connected by the orbit, one corresponding to the forward asymptotic time and the other to the reverse asymptotic time limit, i.e., $x(t) \rightarrow x_1^*$ as $t \rightarrow -\infty$ and $x(t) \rightarrow x_2^*$ as $t \rightarrow \infty$.

The asymptotic values of the solution [Eq. (7)]

$$P(\chi) \rightarrow 1.5748 \text{ as } \chi \rightarrow -\infty$$

and

$$P(\chi) \rightarrow -1.5748 \text{ as } \chi \rightarrow \infty.$$

exactly match with the saddle foci for the particular parametric values, $a = -1.23999$, $b = -\frac{1}{2}$, and thus the corresponding phase curve B' as shown in Fig. 6(a) is heteroclinic orbit. The existence of a heteroclinic orbit connecting the periodic solutions represents the dark soliton [11], which we have shown in Fig. 5(a). We also have shown the shape of the potential function in Fig. 6(b).

Although bright solitons are relatively easy to generate in optical fiber, the dark solitons are less sensitive to optical fiber loss, less influenced by noise, and are more stable

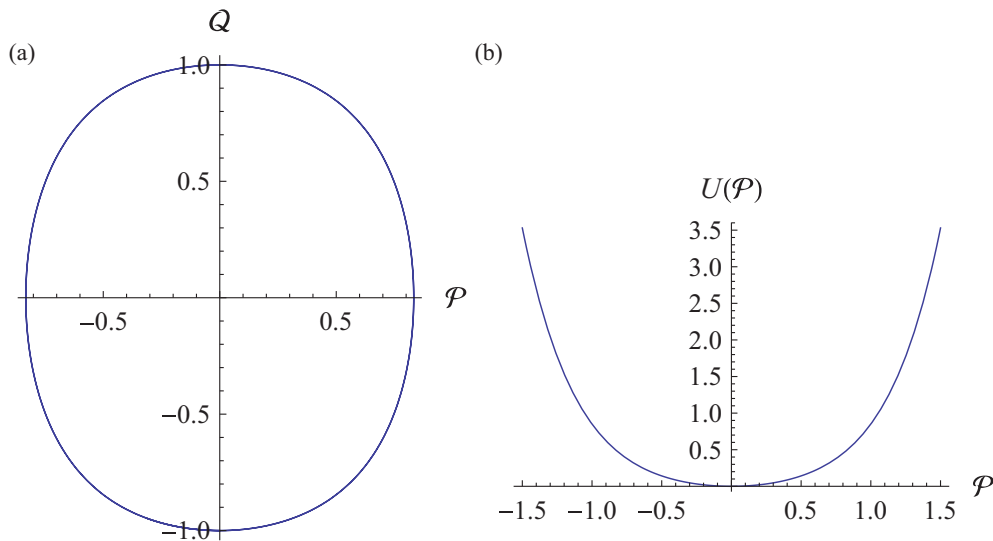


FIG. 4. (Color online) (a) Phase trajectory for the system in Eq. (6). Here, for both plots, we have used the values $a = -1$, $b = \frac{1}{2}$, and $c = \frac{1}{5}$ and (b) shape of the potential function (single-well potential) as computed from Eq. (8).

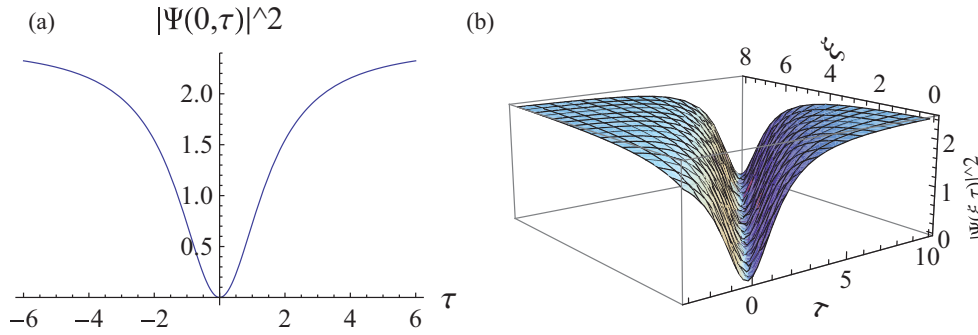


FIG. 5. (Color online) (a) Intensity of the solitary wave profile $|\Psi(0, \tau)|^2$ as a function of τ and its (b) evolution as computed from Eq. (17) for the value $a = v = -1.23999$, $b = -\frac{1}{2}$, and $c = -\frac{b^2}{3a}$.

against Gordon-Haus jitter in long communication line [12]. As the mutual interaction between two neighboring dark solitons is much weaker than that between two bright solitons [13], the properties of the dark soliton attracted scientists in communication systems. But it is difficult to use a dark soliton with a tanh-type wave form in a transmission system because dark pulses cannot be easily generated.

B. Case 2: $\Omega = \frac{1}{3}$

Equation (5b) takes the form

$$(k + \Omega^2 - \Omega^3)\mathcal{P} - (1 - \Omega\alpha_1)\mathcal{P}^3 - (\alpha_3 - \Omega\alpha_4)\mathcal{P}^5 = 0. \quad (19)$$

Setting the coefficients of \mathcal{P} , \mathcal{P}^3 , and \mathcal{P}^5 to zero in Eq. (19) and using $\Omega = \frac{1}{3}$ we obtain $k = -\frac{2}{27}$ and the constraint condition

$$\Omega = \frac{1}{\alpha_1} \quad \text{and} \quad \Omega = \frac{\alpha_3}{\alpha_4}, \quad \text{which implies } \alpha_4 = \alpha_1 \alpha_3. \quad (20)$$

In this case, $\mathcal{P}(\chi)$ satisfies the ordinary differential equation similar to that in (7) but only differs in the coefficient values:

$$(\mathcal{P}_\chi)^2 = a'\mathcal{P}^2 - b'\mathcal{P}^4 - c'\mathcal{P}^6 + 2\mathcal{E}'. \quad (21)$$

In this case, $a' = (v - \frac{1}{3})$, $b' = \frac{9+2\alpha_2}{6}$, $c' = \frac{5\alpha_4+4\alpha_5}{15}$, and \mathcal{E}' is the arbitrary constant of integration. In case 2, similar to Eq. (7) one can solve Eq. (21) to get the bright, dark, and

periodic wave solutions of Eq. (3). Only here the coefficients a' , b' , and c' are different from that in Eq. (7).

IV. DISCUSSION

Before arriving at a conclusion, let us discuss some application of the above theoretical prediction. For large channel-handling capacity in the frame of dense time-domain multiplexing and for high speed, it is necessary to transmit a solitary wave of ultrashort pulses at a high bit rate. At the same time it is also important to consider the higher-order non-Kerr-like nonlinearity including derivative in the HNLS equation for sub-10 fs pulse propagation. The relevance of these terms is also important in the frame of postsoliton compression that can be achieved in highly nonlinear material. Compared to silica glasses, chalcogenide glasses exhibit an extremely high nonlinear refractive-index coefficient that can be two or three orders of magnitude greater than that of silica at $1.55 \mu\text{m}$. They also offer several distinctive optical properties such as a transmission window that extends far into the infrared (IR) spectral region (up to $25 \mu\text{m}$ for telluride glasses). Because of high nonlinearity and large IR transparency, chalcogenide fibers are well suited for compact Raman amplifiers, supercontinuum generation, and other mid-IR sources. For experimental verification of the propagation of solitary wave, one may use the waveguide made of chalcogenide glasses, which are made from heavy chalcogen elements such

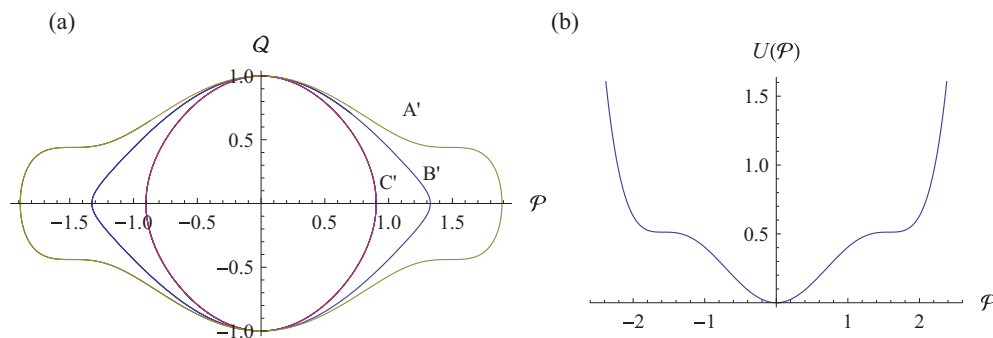


FIG. 6. (Color online) (a) Phase trajectory for the system in Eq. (6). Here we have used the values $a = -1.1$ (A'), $a = -1.23999$ (B'), $a = -1.6$ (C'), $b = -\frac{1}{2}$, and $c = -\frac{b^2}{3a}$ and (b) shape of the potential function as computed from Eq. (8) for $a = -1.23999$, $b = -\frac{1}{2}$, and $c = -\frac{b^2}{3a}$.

as S, As, Se, and Te, having electron shells which are easily polarizable under an electromagnetic field excitation. For example, the chalcogenide glass As_2Se_3 , the nonlinear index coefficients [14,15] are $n_2 = 2.2 \times 10^{-17} \text{ m}^2/\text{W}$ and $n_4 = -6.5 \times 10^{-31} \text{ m}^4/\text{W}^2$ and for the As_2S_3 sample, the values are $n_2 = 4.2 \times 10^{-18} \text{ m}^2/\text{W}$ and $n_4 = -6.0 \times 10^{-32} \text{ m}^4/\text{W}^2$. In general, the nonlinear coefficients γ_i ($i = 1, 2$) can be estimated from $\gamma_i = \frac{2\pi n_j}{\lambda A_{\text{eff}}}$, where n_j ($j = 2, 4$) are the nonlinear refractive index coefficient. Here $A_{\text{eff}} = \pi w^2$ is the effective fiber core area, where w is the core radius of the fiber, which varies from 3 to 3.8 μm for As_2Se_3 and 1.3 to 1.7 μm for As_2S_3 . λ , the typical telecommunication wavelength, is 1.55 μm . For the range of cubic nonlinear coefficient $|\gamma_1| = 2000\text{--}3000 \text{ W}^{-1}/\text{km}$, we have calculated the values for quintic nonlinear coefficients: $|\gamma_2| = 1.3\text{--}3 \text{ W}^{-2}/\text{km}$ for As_2Se_3 and $|\gamma_2| = 3.3\text{--}7.6 \text{ W}^{-2}/\text{km}$ for As_2S_3 respectively. The 1.55 μm window is mainly of interest for long-distance telecommunication application. The other important feature of this transmitted wavelength is that it matches the fiber's low-loss regions. Fiber energy loss (absorption) compensation with sufficient Raman gain and distortionless propagation of picosecond soliton pulses in a monomodal optical fiber have been experimentally demonstrated by Mollenauer *et al.* [16]. Chalcogenide glasses have attracted much interest in the last few years as a nonlinear optical material in the telecommunication wavelength window of 1550 nm and are promising candidates for planar nonlinear optical (NLO) rib waveguide devices due to high nonlinearity, high refractive index, and nonlinear optical losses (0.05 dB/cm) at 1550 nm [17,18]. In a very recent work, El-Amraoui *et al.* [19] measured the fiber losses as low as 0.35 dB/m at 1.55 μm for a 45-m-long 2.3 μm core size fiber. The related nonlinear Kerr coefficient is estimated as high as $2750 \text{ W}^{-1}\text{km}^{-1}$. It is also important to note the fact that chalcogenide glasses exhibit the highest nonlinear refractive indices and suffer, at worst, only moderately from two-photon absorption. Also they do not suffer from free-carrier absorption. The nonlinear absorption faced by the fiber material can be compensated using derivative higher-order nonlinear Raman gain terms. In this context, Tuniz *et al.* [20] studied how Raman gain and nonlinear absorption counteract across the C and L bands in two-photon absorption effects in single-mode chalcogenide fiber.

Now, physically, for the ultrashort laser pulse propagation through optical fiber at telecommunication wavelength 1.55 μm (see the last reference of Ref. [2]) and carrier frequency $\omega_0 = 1.22 \times 10^{15} \text{ s}^{-1}$, i.e., $T_0 = 5.1475 \times 10^{-15} \text{ s}$, if we choose the typical real experimental value for the model parameters of Eq. (2) as $a_1 = \frac{\beta_2}{2} = 10 \text{ ps}^2/\text{km}$, $a_2 = \gamma_1 = 2765 \text{ W}^{-1}/\text{km}$, $a_3 = \frac{\beta_3}{6} = 0.0235 \text{ ps}^3/\text{km}$, $a_4 = -\frac{\gamma_1}{\omega_0} = -14.2328 \text{ W}^{-1}/[(2\pi)\text{km THz}]$, and $a_5 = \gamma_1 T_R = 14931 \text{ W}^{-1} \text{ fs}/\text{km}$ ($T_R = 5.4 \text{ fs}$ for chalcogenide glass fiber [15]), we can estimate the size of the coefficients of the non-Kerr nonlinearities of Eq. (2) from the constraint relations in Eq. (13). The calculated values for the coefficients of non-Kerr nonlinearities are $a_6 = \gamma_2 = \frac{3a_2^2 a_3}{5a_1^3} = 2.533 \text{ W}^{-2}/\text{km}$, $a_7 = \frac{3a_2 a_3^2 a_4}{5a_1^3} = -1.304 \times 10^{-2} \text{ W}^{-2}/[(2\pi)\text{km THz}]$, and $a_8 = \frac{a_2 a_3^2 a_5}{2a_1^3} = 11.3996 \text{ W}^{-2} \text{ fs}/\text{km}$. For the sub-10 fs bright pulse

communication in a non-Kerr medium with the above model parameter values for Eq. (2), one can check that we need chalcogenide optical fiber of the type As_2Se_3 of core radius 3.20415 μm and for As_2S_3 of core radius 1.399 μm respectively. If we use the same parameter values for the dark pulse propagation, one can obtain the energy value for a dark pulse as $\mathcal{E} = -\frac{a^2}{6b} = -\frac{(v-2\Omega+3\Omega^2)^2}{3\alpha_1+2\alpha_2} = -88.779$.

V. CONCLUSION

In conclusion, we have reported optical bright and dark solitary wave solutions of higher-order nonlinear Schrödinger equation in the presence of non-Kerr terms subject to constraint relations among the parameters. The derivative Kerr and non-Kerr nonlinear terms are important for compensation of the nonlinear absorption during propagation in highly nonlinear materials. These terms also play an important role for the post-soliton compression to get highly stable compressed optical pulses. We also have presented the periodic solutions, which are very meaningful in optics. We followed the dynamical systems theoretic approach to study qualitatively the existence of bright, dark, and periodic solitary wave solutions. We presented the phase space behavior of the solutions together with their existence curves such as homoclinic, heteroclinic, and periodic orbits. We have seen that the estimated values for non-Kerr nonlinear model parameters of Eq. (2) agreed with those of the waveguide made of chalcogenide glasses. So the inclusion of the non-Kerr nonlinear terms in Eq. (1) is really needed to describe the sub-10 fs pulse propagation in highly nonlinear optical fiber. As in case 1, we have checked the parametric condition in Eq. (21) for case 2 using the model parameters given above. The quintic non-Kerr nonlinear terms in contemporary optics have become very crucial to upcoming applications in ultrafast signal routing systems, double doped optical fiber, optical switching, etc. The periodic solution can be used to study the formation of solitons in the periodic structure if one considers the quintic non-Kerr nonlinearity in a fiber Bragg grating [21]. Finally, with the calculated parameter values for highly nonlinear optical fiber made of chalcogenide glasses, the HNLS equation, in the presence of non-Kerr nonlinear terms as a higher-order perturbation, not only could find application in broadband telecommunication that extends far into the infrared (IR) spectral region for the bright and dark optical pulses, but also Eq. (2) may be a new model equation for experimental designing sub-10 fs optical pulse propagation, which will be applicable for the next generation optical fiber using chalcogenide-type highly nonlinear optical glasses. Finally, our study may provide us with the possibility to explore physical phenomena with the help of laser spectroscopic techniques and ultrashort laser pulses technology to understand the most basic properties which determine the dynamic response of materials in femtosecond resolution.

ACKNOWLEDGMENT

A.C. is deeply indebted to Dr. Philippe Grelu, Professor of Physics and Optoelectronics at the University de Bourgogne (Dijon, France), for constructive discussions.

- [1] A. Hasegawa and F. Tappert, *Appl. Phys. Lett.* **23**, 142 (1973).
- [2] N. Sasa and J. Satsuma, *J. Phys. Soc. Jpn.* **60**, 409 (1991); Y. Kodama and A. Hasegawa, *IEEE J. Quantum Electron.* **23**, 5610 (1987); A. Hasegawa and Y. Kodama, *Solitons in Optical Communications* (Clarendon Press, Oxford, 1995); G. P. Agrawal, *Nonlinear Fiber Optics* (Academic Press, New York, 1995).
- [3] G. P. Agrawal, *Nonlinear Fiber Optics*, 4th ed. (Academic Press, New York, 2006).
- [4] K. Porsezian and K. Nakkeeran, *Phys. Rev. Lett.* **76**, 3955 (1996); M. Gedalin, T. C. Scott, and Y. B. Band, *ibid.* **78**, 448 (1997); S. L. Palacios, A. Guinea, J. M. Fernández-Díaz, and R. D. Crespo, *Phys. Rev. E* **60**, R45 (1999); Z. Li, L. Li, H. Tian, and G. Zhou, *Phys. Rev. Lett.* **84**, 4096 (2000).
- [5] R. Radhakrishnan, A. Kundu, and M. Lakshmanan, *Phys. Rev. E* **60**, 3314 (1999).
- [6] S. Hädrich, J. Rothhardt, M. Krebs, F. Tavella, A. Willner, J. Limpert, and A. Tünnermann, *Optics Express* **18**, 0242 (2010); Y. Song, C. Kim, K. Jung, H. Kim, and J. Kim, *ibid.* **19**, 14518 (2011).
- [7] A. Choudhuri and K. Porsezian, *Opt. Commun.* **285**, 364 (2012).
- [8] A. Choudhuri and K. Porsezian, *Phys. Rev. A* **85**, 033820 (2012).
- [9] H. Triki and T. R. Taha, *Math. Comput. Sim.* **82**, 1333 (2012).
- [10] K. T. Alligood, T. Sauer, and J. A. Yorke, *Chaos: An Introduction to Dynamical Systems* (Springer, New York, 1997).
- [11] J. Belmonte-Beitia, *Math. Meth. Appl. Sci.* **36**, 974 (2013).
- [12] S. Yu. Kivshar, M. Haelterman, Ph. Emplit, and J. P. Hamaide, *Opt. Lett.* **19**, 19 (1994).
- [13] W. Zhao and E. Bourkoff, *Opt. Lett.* **14**, 1371 (1989).
- [14] G. Boudebs, S. Cheru Kulappurath, H. Leblond, J. Troles, F. Smektala, and F. Sanchez, *Opt. Commun.* **219**, 427 (2003); A. Zakery and S. R. Elliott, *Optical Nonlinearities in Chalcogenide Glasses and Their Applications*, Vol. 135 (Springer, Berlin, 2007).
- [15] B. Ung and M. Skorobogatiy, *Opt. Express* **18**, 8647 (2010); R. E. Slusher, G. Lenz, J. Hodelin, J. Sanghera, L. B. Shaw, and I. D. Aggarwal, *J. Opt. Soc. Am. B* **21**, 1146 (2004).
- [16] L. F. Mollenauer, R. H. Stolen, and M. N. Islam, *Opt. Lett.* **10**, 229 (1985).
- [17] J. T. Gopinath, M. Soljačić, E. P. Ippen, V. N. Fuflyigin, W. A. King, and M. Shurgalin, *J. Appl. Phys.* **96**, 6931 (2004).
- [18] S. J. Madden, D.-Y. Choi, D. A. Bulla, A. V. Rode, B. Luther-Davies, V. G. Ta'eed, M. D. Pelusi, and B. J. Eggleton, *Opt. Express* **15**, 14414 (2007).
- [19] M. El-Amraoui, J. Fatome, J. C. Jules, B. Kibler, G. Gadret, C. Fortier, F. Smektala, I. Skripatchev, C. F. Polacchini, Y. Messaddeq, J. Troles, L. Brilland, M. Szpulak, and G. Renversez, *Opt. Express* **18**, 4547 (2010).
- [20] A. Tuniz, G. Brawley, D. J. Moss, and B. J. Eggleton, *Opt. Express* **16**, 18524 (2008).
- [21] K. Porsezian, K. Senthilnathan, and S. Devipriya, *IEEE J. Quantum Electron.* **41**, 789 (2005).